Abnormal development of Purkinje cells and lymphocytes in *Atm* mutant mice

Paul R. Borghesani*†‡, Frederick W. Alt§¶‖, Andrea Bottaro¶‖††, Laurie Davidson§¶, Saime Aksoy‡‡, Gary A. Rathbun¶‖, Thomas M. Roberts‡‡, Wojciech Swat¶‖, Rosalind A. Segal*†, and Yansong Gu‡§¶**

*Department of Pediatric Oncology and ‡‡Division of Cellular and Molecular Biology, Dana–Farber Cancer Institute; §Howard Hughes Medical Institute and The Children's Hospital; ¶The Center for Blood Research; Departments of †Neurobiology and ‖Genetics, Harvard Medical School, Boston, MA 02115

Contributed by Frederick W. Alt, December 28, 1999

Motor incoordination, immune deficiencies, and an increased risk of cancer are the characteristic features of the hereditary disease ataxia–telangiectasia (A-T), which is caused by mutations in the *ATM* gene. Through gene targeting, we have generated a line of *Atm* mutant mice, $Atm^{y/y}$ mice. In contrast to other *Atm* mutant mice, $Atm^{y/y}$ mice show a lower incidence of thymic lymphoma and survive beyond a few months of age. $Atm^{y/y}$ mice exhibit deficits in motor learning indicative of cerebellar dysfunction. Even though we found no gross cerebellar degeneration in older $Atm^{y/y}$ animals, ectopic and abnormally differentiated Purkinje cells were apparent in mutant mice of all ages. These findings establish that some neuropathological abnormalities seen in A-T patients also are present in *Atm* mutant mice. In addition, we report a previously unrecognized effect of *Atm* deficiency on development or maintenance of $CD4^+8^+$ thymocytes. We discuss these findings in the context of the hypothesis that abnormal development of Purkinje cells and lymphocytes contributes to the pathogenesis of A-T.

The autosomal recessive disease ataxia–telangiectasia (A-T) is characterized by the early onset of progressive ataxia, ocular telangiectasias, and susceptibility to infections and tumors (1, 2). A-T is caused by mutations in the *ATM* gene (3). The *ATM* protein encodes a serine/threonine kinase and induces *p53*, c-*Abl*, and *Brca1* activation after DNA damage (4–8). *ATM*-deficient cells exhibit cell-cycle checkpoint defects, resulting in hypersensitivity to genotoxic stress (9). However, it is less clear whether the abnormal cellular physiology of various *ATM*-deficient cell types also results from defective DNA repair. For example, potassium-mediated depolarization is attenuated in A-T fibroblasts (10), and calcium mobilization and phospholipase-Cγ activation are reduced in A-T B cells after antigen receptor stimulation (11). Altered cellular physiology may independently contribute to the clinical manifestations of A-T.

Several lines of *Atm* mutant mice recapitulate numerous aspects of A-T (12–15). These *Atm* mutant mice exhibit growth retardation, immune system defects including defects in T cell maturation, germ cell dysfunction, and increased sensitivity to ionizing radiation (IR). Although behavioral abnormalities were observed (14), altered cerebellar histology or degeneration was not reported (12–15). The diversity of *ATM* mutations and the variability in the clinical progression of A-T raises questions concerning how individual *ATM* mutations and genetic factors contribute to the clinical severity of A-T. Likewise, independently generated *Atm*-deficient mice may also vary in their phenotypic manifestations, reflecting mutagenesis strategies and/or genetic backgrounds.

Murine *Atm* is expressed in both embryonic and adult tissues and likely functions at multiple developmental stages (16). It remains unclear whether *Atm* deficiency alters developmental processes and how this may contribute to neurodegeneration and immunodeficiency in A-T patients. Clinical studies documenting the early onset of ataxia (17–19) and early abnormalities in Purkinje cell morphology and localization (20, 21) support the hypothesis that *ATM* function is essential for normal cerebellar development. To further evaluate the potential *Atm* functions, we have generated and characterized a line of *Atm* mutant mice.

Materials and Methods

Generation of $Atm^{y/y}$ Mice. *Atm* genomic clones were isolated from a 129/Sv mouse genomic library (Stratagene). Exons encoding the RAD3- and phosphatidylinositol 3-kinase-homology domains were characterized, and those encoding amino acids 7279–7818 (22) were replaced by a neomycin-resistance (*neo*^{r}) gene in a reverse orientation. The *Sal*I-linearized construct was electroporated into J1 embryonic stem (ES) cells (a gift from R. Jaenisch, Massachusetts Institute of Technology), and $Atm^{+/y}$ ES cells were identified by Southern blot analysis of G418- and ganciclovir-selected ES clones. $Atm^{+/y}$ ES cells were used to generate $Atm^{+/y}$ mice. Subsequent breedings in a pathogen-free facility generated the $Atm^{y/y}$ strain in a 129Sv/C57B6 mixed background.

Western Blot Analysis. Tissues were lysed by using standard techniques, and 20 μg of protein per lane was separated by SDS/5–10% PAGE and transferred to poly(vinylidene difluoride) membranes (NEN). Monoclonal antibody ATM-2C1 (GeneTex, San Antonio, TX) was raised against a human ATM fragment (amino acids 2577–3056) and crossreacts with murine Atm. ATM-N1 was raised by immunizing New Zealand White rabbits with a mixture of two peptides, N1 (ATM residues 16–31) and N2 (ATM residues 41–56) and affinity purified using the N2 peptide. Both antibodies were used at a 1:800 dilution in PBS. Control human cell lines were obtained from the National Institute of General Medical Sciences cell repository [GM02184D (control) and GM01526E (A-T)]

FACS Analysis. Single-cell suspensions were prepared from lymphoid organs, stained with antibodies, and analyzed on a FACScalibur flow cytometer (Becton Dickinson). Antibodies (PharMingen) conjugated with FITC, phycoerythrin (PE)-RM4–5, biotin (bi), or CyChrome (CyC) were used: anti-B220-CyC, anti-CD43-PE, anti-IgM-FITC, anti-IgD-bi, anti-CD4-PE, anti-CD8-CyC, anti-CD3ε-FITC, and anti-TCRβ-FITC. The data were analyzed with CELLQUEST (Becton Dickinson).

Behavioral Analysis. Open-field exploration was assessed by counting the number of 1.5 × 1.5-inch grids covered in 2 min

Abbreviations: A-T, ataxia–telangiectasia; IR, ionizing radiation; ES, embryonic stem; RT, reverse transcription; DN, double negative; DP, double positive; SP, single positive; TCR, T cell receptor.

‡P.R.B. and Y.G. contributed equally to this work.

**To whom reprint requests should be addressed. E-mail: alt@rascal.med.harvard.edu.

††Present address: University of Rochester Medical Center, Department of Medicine, Immunological Unit, Rochester, NY 14642.

The publication costs of this article were defrayed in part by page charge payment. This article must therefore be hereby marked "*advertisement*" in accordance with 18 U.S.C. §1734 solely to indicate this fact.

Article published online before print: *Proc. Natl. Acad. Sci. USA*, 10.1073/pnas.050584897. Article and publication date are at www.pnas.org/cgi/doi/10.1073/pnas.050584897

within a 1-m^2 box. Wild-type and *Atm*$^{y/y}$ littermates were tested on an accelerating rotating rod (Columbia Instruments, OH), with two or three sets of five trials each day for 7 days. The 4-cm diameter running bar was covered with masking tape and accelerated at 30 revolutions per min^2. The average age of the mutant and wild-type populations was the same (8.8 mo; range, 6 to 10 mo). The populations differed in the average weight (wild-type, 37.9 ± 2.6 g; *Atm*$^{y/y}$, 30.6 ± 1.8 g) and gender distribution (wild-type female:male, 4:5; *Atm*$^{y/y}$, 8:5). Post-hoc analysis indicated that the difference in motor learning seen between wild-type and *Atm*$^{y/y}$ mice is irrespective of animal weight or gender.

Immunohistochemistry. Mice were anesthetized and perfused with 1.5 body volumes of 4% paraformaldehyde in 100 mM phosphate buffer (pH 7.4), postfixed at 4°C for 16 h, and cryoprotected in sucrose, and 16-μm parasagittal sections were cut on a cryostat. Only midsagittal sections were used. Overnight incubations were done with anti-parvalbumin (1:500; Sigma) or anti-calbindin (1:1,000; Sigma) in PBS with 5% goat serum and 0.1% Nonidet P-40 followed by a 2-h incubation with a Cy3-linked goat anti-mouse antibody (1:100; The Jackson Laboratory). Lucifer yellow dye filling was performed as described (23), allowing 12 min for each cell to fill.

Quantitation. Using 11-mo-old littermates, the length of Purkinje cell stem dendrite prior to bifurcation and cell body size from 35 wild-type cells from two animals, and 26 *Atm*$^{y/y}$ cells from three animals were measured in photographs of dye-injected cells by a blinded observer. Molecular layer thickness was measured in Nissl- or calbindin-stained sections along the third, sixth, and ninth folia halfway down the preculminate, primary, and secondary fissures, respectively, in three nonadjacent midsagittal sections. Ectopic Purkinje cells were counted in nonadjacent midsagittal sections (8–12 sections per animal) double-labeled by calbindin immunostaining and propidium iodide. Purkinje cell numbers were counted in six to nine nonadjacent hematoxylin and eosin-stained 16-μm sections in the anterior, central, and posterior lobule along the third, sixth, and ninth folia, respectively.

Results

Generation of the *Atm*$^{y/y}$ Strain. An *Atm* mutation, *Atm*^{y}, was created by replacing the Rad-3 homology domain (corresponding to exons 50–52 of human *ATM*; ref. 24) with a *neo*^{r} gene in murine ES cells (Fig. 1*A*). This mutation, which is distinct from previously generated *Atm* mutations (see Fig. 1*A*), was transmitted into mice (Fig. 1*B*). *Atm*$^{+/y}$ mice appeared indistinguishable from controls; however, *Atm*$^{y/y}$ mice shared a number of characteristics previously observed in young *Atm* mutant mice, including growth retardation (≈80% weight of wild-type), infertility, immunodeficiency, and frequent thymic lymphomas (refs. 13–15; see below). Additionally, *Atm*$^{y/y}$ ES cells were hypersensitive to IR (data not shown).

Sequence analysis of reverse transcription (RT)-PCR products from *Atm*$^{y/y}$ tissues revealed that the *Atm*$^{y/y}$ mutation allows for production of at least two alternative transcripts (*Atm*^{y} transcripts I and II; Fig. 1*A*). The *Atm*^{y} transcript I includes 494 bp of a reverse-oriented *neo*^{r} gene, which replaces 536 bp of *Atm* exons 50–52. This type of transcript, a read-through of the *neo*^{r} gene after a deletion/replacement, has been previously observed (25). In *Atm*^{y} transcript I, splicing of exon 49 to this exogenous exon results in a frameshift and a stop codon (Fig. 1*A*). In *Atm*^{y} transcript II, exon 49 is directly spliced to exon 53, leading to an in-frame fusion, theoretically allowing for production of an *Atm*^{y} protein with an intact phosphatidylinositol 3-kinase domain. Although these aberrant transcripts can be detected by RT-PCR in *Atm*$^{y/y}$ tissues, full-length *Atm*^{y} transcripts were not detectable by Northern blot analysis (Fig. 1*C*). Furthermore, neither full-length nor partial *Atm*-immunoreactive protein bands were detected in the *Atm*$^{y/y}$ tissues by using either N-terminal or C-terminal antibodies (Fig. 1 *D–G*; see legend); although we

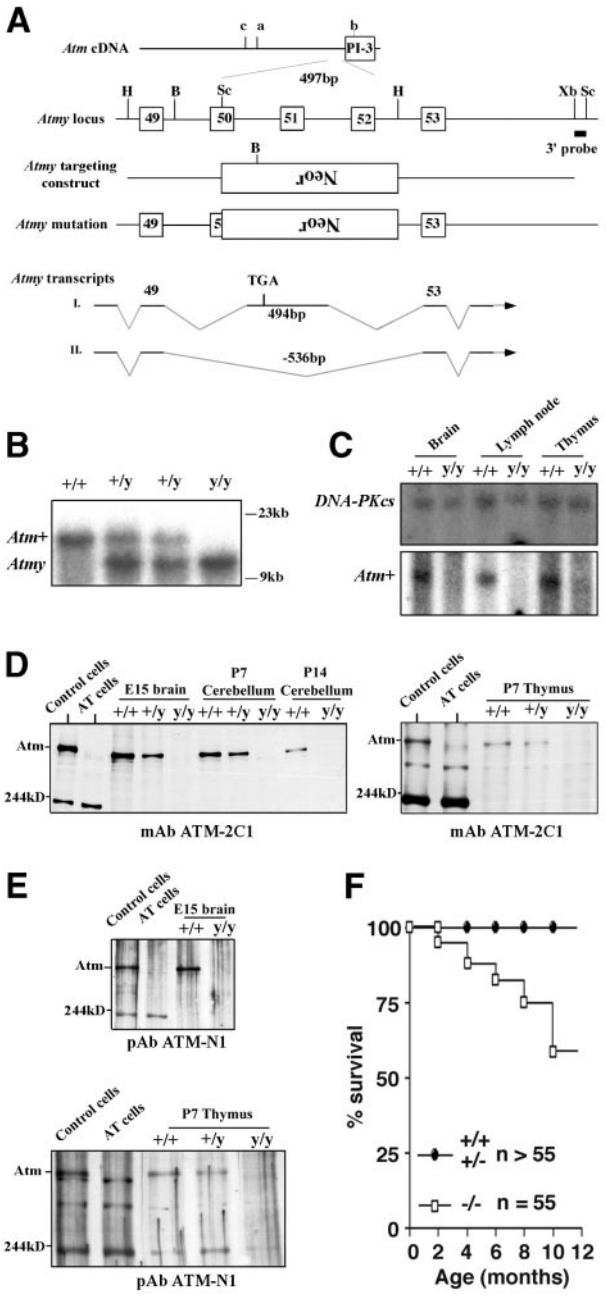

Fig. 1. Generation of *Atm*$^{y/y}$ mice and *Atm* expression. (*A*) Location of the *Atm*^{y} mutation and other reported murine *Atm* mutations; a (14), b (15, 16), and c (13). B, *Bam*HI; H, *Hin*dIII; Bg, *Bgl*II; Sc, *Sac*I; Xb, *Xba*I; and Neo^r, neomycin-resistance gene. (*B*) Southern blot analysis of *Atm*^{y} mutation. *Bam*HI-digested DNA is probed with the indicated 3′ probe (*A*). (*C*) Northern blot analysis of *Atm* expression. Total RNA from brain, lymph node, and thymus of wild-type (+/+) and *Atm*$^{y/y}$ (y/y) mice were probed with an *Atm* cDNA fragment (*Lower*) and reprobed with a *DNA-PKcs* cDNA probe (*Upper*) to confirm equal RNA loading. (*D* and *E*) Western blot analysis of *Atm* expression in *Atm*$^{y/y}$ tissues using antibodies raised against the C terminus (*D*) and N terminus (*E*) of the *ATM* protein. The bands at ≈200 kDa and ≈300 kDa are likely nonspecific since they are present in human and murine samples of both genotypes. (*F*) Kaplan–Meier survival curve of *Atm*$^{y/y}$ mice (n = 55).

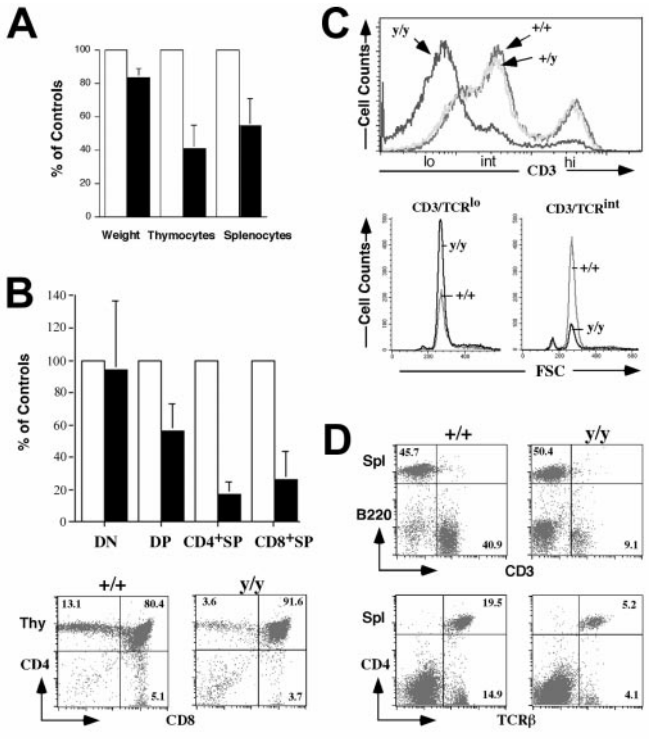

Fig. 2. Abnormal T lymphocyte development in *Atm*$^{y/y}$ mice. (*A*) Average pairwise comparisons of weight, total numbers of thymocytes, and splenocytes from 10 same-sex littermates pairs 1–5 mo old. (*B*) (*Upper*) The average reduction of the total number of each *Atm*$^{y/y}$ thymocyte subpopulations (DN, CD4$^-$8$^-$; DP; CD4$^+$8$^+$; CD4$^+$SP, CD4$^+$8$^-$; CD8$^+$SP, CD4$^-$8$^+$) from seven littermate pairs. (*Lower*) FACS analysis of T cell development in *Atm*$^{y/y}$ thymuses. (*C*) Histogram of CD3 surface expression in *Atm*$^{y/y}$ thymocytes (y/y). (*Lower*) FSC (forward site scatter) using a lymphocyte gate on CD3^{low} and CD3^{int} DP cells, respectively. (*D*) Splenic T cells in *Atm*$^{y/y}$ mice (y/y) were reduced in numbers, but their surface phenotype (TCRβ/CD3 expression) appeared to be normal. Numbers indicate the percentage of splenic T cells (CD3$^+$) and B cells (B220$^+$).

cannot rule out low-level expression of an altered *Atm* protein. In this context, we did detect a slow migrating *Atm* immunoreactive protein in one *Atm*$^{y/y}$ ES cell line (data not shown).

Tumorigenesis and Lifespan. Long-term assessment of previously generated *Atm* mutant mice was compromised by early development of thymic lymphomas, causing death uniformly by 4 or 5 mo of age (13–15). *Atm*$^{y/y}$ mice also succumb to thymic lymphomas; however, over 50% survived for 10 mo or more (Fig. 1*H*). Based on surface marker expression, lymphomas in *Atm*$^{y/y}$ mice were generally T cell lineage in origin (data not shown), as observed previously for other *Atm* mutant mice (13–15). Of note, it was recently demonstrated that breeding an *Atm*-deficient line into a recombinase activating gene-1 (*RAG-1*)-deficient background prevented the formation of T cell lymphomas in that line and resulted in increased survival (32).

Abnormalities of the Immune System. As previously reported for other strains of *Atm*-deficient mice, we observed a disproportionate reduction (≈40–50% of normal levels) in thymocyte and splenocyte numbers, as compared with the ≈20% reduction in body weight, in *Atm*$^{y/y}$ mice (Fig. 2*A*).

To identify defects in *Atm*$^{y/y}$ lymphocyte development, we examined thymocyte subsets by flow cytometry (Fig. 2 *B* and *C*). Rearrangement and expression of T cell receptor (TCR)β genes in CD4$^-$8$^-$ (double negative, DN) thymocytes leads to their differentiation into CD4$^+$8$^+$ (double positive, DP) cells (26). This process, as well as expansion of DP cell numbers and initiation of TCRα gene rearrangement, requires signaling by the pre-TCR complex (composed of pre-Tα chains, TCRβ, and CD3), which is expressed at low levels on "early" DP (CD3^{low} DP) thymocytes (26). Following TCRα gene rearrangement and expression in DP thymocytes, CD3 surface expression increases during the transition of CD3^{low} DP cells to CD3^{int} cells, which express CD3 in the context of $\alpha\beta$TCR. Such CD3^{int} DP cells can undergo negative selection or programmed cell death; alternatively, they can be rescued by positive selection and mature into single positive (SP) thymocytes and peripheral T cells that express higher levels of CD3/$\alpha\beta$TCR receptors (26).

Our preliminary studies revealed no obvious abnormalities with respect to the various DN subpopulations in *Atm*$^{y/y}$ vs. wild-type mice, as judged by expression of the CD25 and CD44 surface markers (W.S. and Y.G., unpublished data). However, there was a 2-fold decrease in DP thymocyte numbers and a 5-fold decrease in SP thymocyte numbers in *Atm*$^{y/y}$ thymuses (Fig. 2*B*). These findings generally agree with previous studies that implicated a defect in maturation of DP to SP thymocytes in association with the *Atm* deficiency (13–15). To further pinpoint the developmental stage disrupted by the *Atm*^{y} mutation, we carefully analyzed CD3 expression in the different DP and SP populations. Strikingly, the majority of *Atm*$^{y/y}$ DP thymocytes expressed low CD3 levels, in contrast to intermediate CD3 levels expressed by the majority of wild-type or heterozygous DP cells (Fig. 2*C*; confirmed by specific gating, data not shown). Scatter analyses of individual populations of *Atm*$^{y/y}$ and wild-type DP thymocytes revealed no major differences in cell size (Fig. 2*C*). Furthermore, despite decreased numbers, gating on SP thymocytes in *Atm*$^{y/y}$ mice demonstrated wild-type levels of CD3 expression (data not shown), indicating that they had undergone positive selection. Likewise, although splenic T cell numbers were reduced by approximately 8- to 10-fold, their surface phenotype appeared normal (Fig. 2 *A* and *D*).

As previously observed in other *Atm* mutant mice (15), the precursor B cell and immature B cell populations were decreased in bone marrow of *Atm*$^{y/y}$ mice, but the numbers of B220-positive and IgM-positive splenic B cells were relatively similar (data not shown). Thus, as previously observed in A-T patients and *Atm* mutant mice (13–15, 27, 28), the accumulation of splenic T cells in *Atm*$^{y/y}$ mice appears more profoundly affected than that of B cells (Fig. 2*D*).

Motor Coordination Deficits. A-T patients suffer from the onset of ataxia during the first few years of life, suggesting that cerebellar function may be compromised prior to Purkinje cell degeneration (17–19). Although *Atm*$^{y/y}$ mice from 4 to 12 months of age tend to explore an open field less than controls [grids crossed by wild-type (n = 10) = 101 ± 47 and *Atm*$^{y/y}$ (n = 17) = 67 ± 41, P = 0.062 by a two-sided t test, see also ref. 14], they do not exhibit ataxia as assessed by paw-prints and bridge crossing (data not shown). As a more sensitive assay of cerebellar function, we tested motor learning on an accelerating rotating rod (Fig. 3*A*). On the first trial day, *Atm*$^{y/y}$ mice (n = 13) performed as well as wild-type mice (n = 9). However, unlike wild-type mice, *Atm*$^{y/y}$ mice failed to improve with repeated trials. After 1 wk of daily training, wild-type mice were performing significantly better than *Atm*$^{y/y}$ mice (Fig. 3*A*). Thus, 4- to 12-mo-old *Atm*$^{y/y}$ mice display mild deficits in motor learning consistent with cerebellar dysfunction.

Cerebellar Pathology. The cerebellar cortex consists of three layers: an outer molecular layer containing Purkinje cell dendrites arranged in parasagittal fans, a single cell layer of Purkinje cell bodies, and the internal granule cell layer containing the small granule neurons. Immunostaining of Purkinje cells with an anti-calbindin antibody and Bodian staining of midsagittal cer-

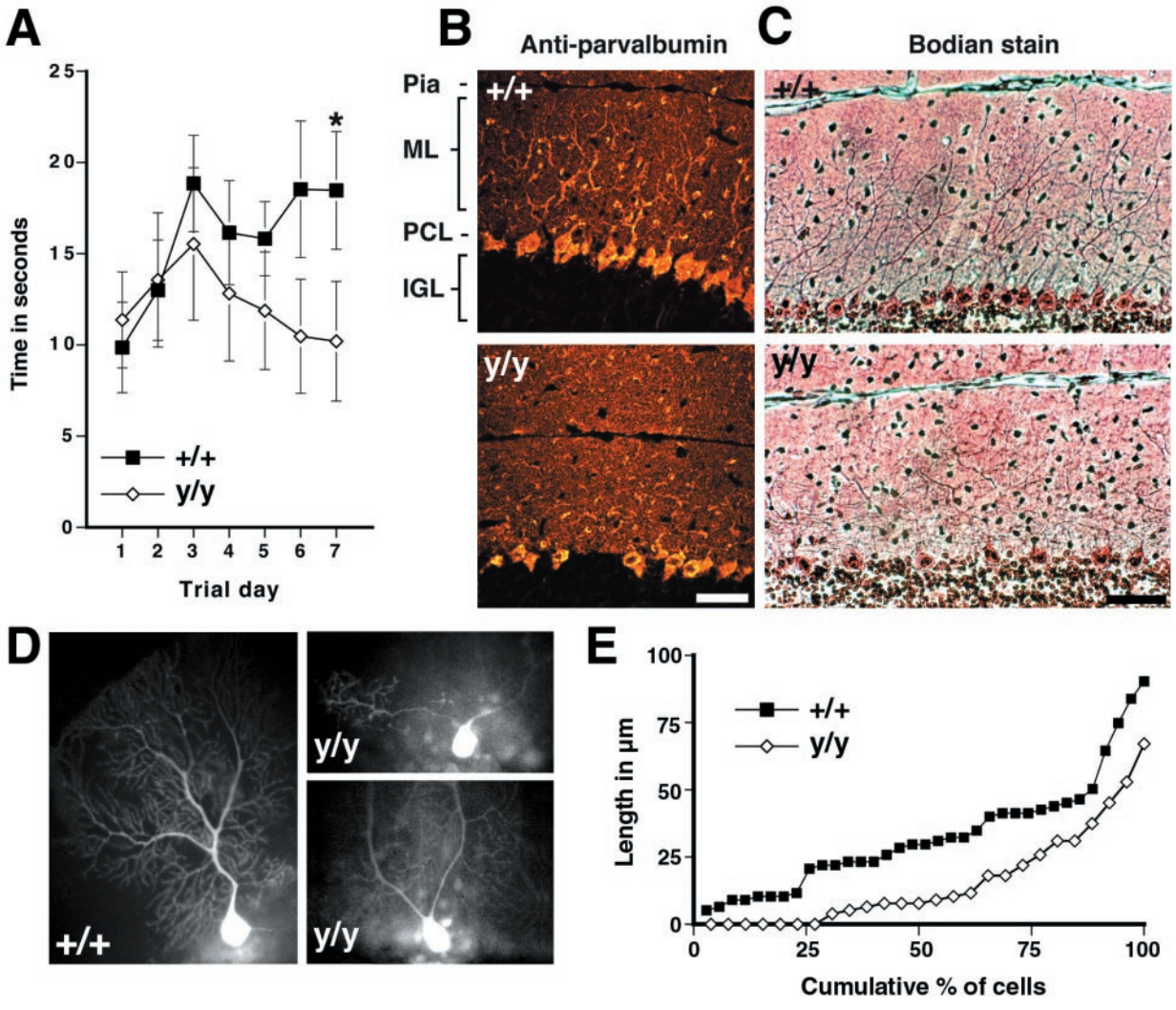

Fig. 3. Motor-learning deficits and dendritic changes in $Atm^{y/y}$ mice. (*A*) Performance of wild-type mice but not $Atm^{y/y}$ mice on an accelerating rotating rod improved over the trial period ($P < 0.01$ by repeated-measure ANOVA, regression slope = 1.21 s/day, $P < 0.05$), and by the seventh trial day, wild-type mice performed better than $Atm^{y/y}$ mice ($P < 0.02$, Mann–Whitney rank sum test). (*B*) Parvalbumin immunohistochemistry of midsagittal cerebellar sections from 5-mo-old wild-type (*Upper*) and $Atm^{y/y}$ mice (*Lower*) reveals the altered dendritic arborization of Purkinje cells in $Atm^{y/y}$ mice. (*C*) This can also be observed in Bodian-stained sections from 1-yr-old mice, wild-type (*Upper*), and $Atm^{y/y}$ (*Lower*). (*D*) Lucifer yellow-injected wild-type and $Atm^{y/y}$ Purkinje cells displaying either the prototypic morphology (+/+) or premature dendritic branching (y/y), which can result in multiple dendrites emanating from the soma (upper y/y cell). (*E*) Cumulative percent graph of stem dendrite length; 7 of 26 $Atm^{y/y}$ Purkinje cells have multiple dendrites. (Scale bar in *B* and *C* is 50 μm.)

ebellar sections from 4- to 12-mo-old $Atm^{y/y}$ mice revealed an irregular pattern of Purkinje cell dendrites (Fig. 3 *B* and *C*, nine age-matched pairs examined). To visualize individual dendritic trees, the fluorescent dye Lucifer yellow was injected into individual $Atm^{y/y}$ and wild-type Purkinje cells of 11-mo-old littermates. As shown, the stem dendrites, which extend from the cell body to the first bifurcation, consistently branch prematurely in $Atm^{y/y}$ mice (Fig. 3 *D–G*, average length in = 16.1 ± 3.6 μm; wild-type = 33.0 ± 3.6 μm, $P < 0.002$ by two-sided *t* test). In addition, dye-injected $Atm^{y/y}$ Purkinje cells often had multiple dendrites originating directly from the cell bodies (Fig. 3*D*), whereas a single large stem dendrite emanated from each wild-type Purkinje cell soma (wild type, 0 of 35 cells; $Atm^{y/y}$, 7 of 26 cells). Finally, $Atm^{y/y}$ dendrites often projected at odd angles in the molecular layer. These changes in dendritic arborization correlate with a 14% decrease in the thickness of the molecular layer [wild-type ($n = 7$), 172 ± 6 μm; $Atm^{y/y}$ ($n = 8$), 148 ± 1 μm, $P < 0.005$ by two-sided *t* test].

In addition to the dendritic abnormalities, there is an increased number of ectopically located Purkinje cells in the molecular layer of $Atm^{y/y}$ mice [Fig. 4 *A* and *B*; wild-type ($n = 5$), 0.98 per section ($n = 6$), 1.81 per section, $P < 0.05$ by two-sided paired *t* test]. Furthermore, varicosities were observed along some $Atm^{y/y}$ Purkinje cell axons in the internal granule cell layer (Fig. 4*C*). These axonal swellings are small (<5 μm in diameter), similar in appearance to those seen during Purkinje cell development (29), and unlike the large axonal torpedoes seen in A-T (1). Further axonal abnormalities in the white matter tracks and deep nuclei were not detected.

These cerebellar abnormalities could reflect either developmental or degenerative changes. However, abnormal Purkinje cell morphology as assayed by immunohistochemistry (data not shown) reduced molecular layer thickness [wild-type, 171 ± 10 μm ($n = 2$) and $Atm^{y/y}$, 148 ± 2 μm ($n = 3$)], and ectopic Purkinje cells were found in 6-wk-old $Atm^{y/y}$ animals. Additionally, we have not observed gross degeneration of the cerebellum in $Atm^{y/y}$ mice with age. Purkinje cells, which are thought to be the initial cerebellar neurons to degenerate in A-T (30, 31), were present

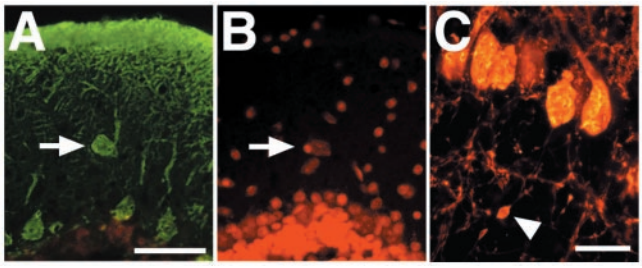

Fig. 4. (*A* and *B*) An ectopic Purkinje cell in an $Atm^{y/y}$ mouse. Ectopic cells were located and counted by double labeling for calbindin immunoreactivity (*A*) and propidium iodide staining (*B*). (*C*) Varicosity along Purkinje cell axon. (Scale bar in *A* is 50 μm and in *C* is 20 μm.)

at a normal density in 11- to 12-mo-old $Atm^{y/y}$ mice (Fig. 4*C* and Table 1), and there was no appreciable increase in the size or number of axonal varicosities in older animals. Thus, the early appearance of abnormal histology and the lack of Purkinje cell loss suggest that cerebellar architecture is disrupted during development in $Atm^{y/y}$ mice.

Discussion

***Atm*$^{y/y}$ Mice Have a Distinct Neurological Phenotype.** $Atm^{y/y}$ mice are growth-retarded, infertile, immunodeficient, and prone to develop thymic lymphomas, attributes similar to those reported for other *Atm* mutant lines (12–15). However, in these previous lines (14, 15), altered cerebellar histology has not been reported, even though behavioral abnormalities were observed (14). In contrast, the $Atm^{y/y}$ mice exhibit two aspects of cerebellar pathology previously reported in A-T patients—ectopic Purkinje cells and abnormal Purkinje cell dendrites—even though there is no evidence for Purkinje cell degeneration in $Atm^{y/y}$ mice up to a year of age. Although $Atm^{y/y}$ mice have a substantially longer lifespan than other reported *Atm* mutant lines (13–15), we see the cerebellar pathology even in young $Atm^{y/y}$ mice. Thus, we currently have no clear-cut explanation for the apparent difference in cerebellar pathology between $Atm^{y/y}$ mice and previously generated *Atm* mutant mice.

The unique cerebellar phenotype and lower incidence of thymic lymphomas in $Atm^{y/y}$ mice suggest that genetic background and/or the mutagenesis strategies employed contribute to the phenotype of murine A-T models. Likewise, the variable progression of A-T may result from different *ATM* mutations compounded with diverse patient genetic backgrounds (1, 2). One possible explanation for the unique phenotype of $Atm^{y/y}$ mice is that an Atm^{y} protein is produced from one of the alternatively spliced Atm^{y} transcripts that we detect in $Atm^{y/y}$ tissues by RT-PCR (Fig. 1*A*). In A-T patients, *ATM* protein fragments are not found in those patients harboring nonsense mutations (33). However, *ATM* protein products have been detected in A-T patients with missense mutations or in-frame deletions (33, 34), and we did detect a slow-migrating Atm immunoreactive protein in one $Atm^{y/y}$ ES cell line (data not shown). Yet, we did not detect *Atm* immunoreactive proteins (using both N-terminal and C-terminal antibodies) in the developing cerebellum and thymus of $Atm^{y/y}$ mice. Thus, while it is possible that a residual amount of aberrant Atm^{y} protein could have eluded detection by our methods, it would appear that *in vivo* expression of such a putative protein is, at most, very low.

Table 1. Purkinje cell survival in 11- to 12-mo-old mice (cells/mm)

Mice	Third folia	Sixth folia	Ninth folia
Wild-type (n = 4)	32.4 ± 1.5	33.9 ± 2.7	25.8 ± 1.1
$Atm^{y/y}$ (n = 4)	31.7 ± 2.9	32.2 ± 1.2	26.9 ± 2.5

Vermial area was the same in both genotypes (ratio of wild-type/$Atm^{y/y}$ area = 0.99).

$Atm^{y/y}$ mice have motor-learning deficits and histological changes in the cerebellum that recapitulate some of the abnormalities seen in A-T patients at early disease stages (20, 21). In particular, abnormal dendritic arborization (Fig. 3) and the presence of ectopic Purkinje cells (Fig. 4), together with a thin molecular layer, are present in $Atm^{y/y}$ mice from age 6 wk to 12 mo. Abnormalities in Purkinje cell localization and morphology in A-T patients could arise early during cerebellar development (21). Alternatively, these could be early manifestations of degeneration (35). We found that ectopic Purkinje cells and reduced molecular layer thickness are apparent in $Atm^{y/y}$ animals at 6 wk of age and do not progress during a year of life. Thus, the neuroarchitectural changes in $Atm^{y/y}$ mice and A-T patients likely reflect altered dendritic arborization during Purkinje cell differentiation, rather than dendrite retraction and degeneration. These dendritic changes could explain our behavioral data in $Atm^{y/y}$ mice (Fig. 3*A*) since dendritic integration of afferent stimuli may be related to arborization (36). Curiously, *Atm*, which is primarily a nuclear protein in dividing cells (37–40), is localized in the cytoplasm and proximal dendrites of developing and mature Purkinje cells (41), suggesting potential functions outside the nucleus during Purkinje cell maturation.

***Atm*$^{y/y}$ Mice Have a Defect in Thymocyte.** Consistent with other *Atm*-deficient mice (13–15), $Atm^{y/y}$ mice have decreased numbers of SP thymocytes and mature T lymphocytes (Fig. 2). However, we find that the population of $CD3^{int}$ cells found in normal mice is drastically reduced in $Atm^{y/y}$ mice, with most $Atm^{y/y}$ DP cells expressing low CD3 levels (Fig. 2*C*). Therefore, our findings indicate that the major thymocyte developmental defect in $Atm^{y/y}$ mice is within the development or maintenance of DP thymocytes, as opposed to the transition from DP to SP thymocytes, as previously suggested for other mutant strains (13–15). However, the mechanism by which *Atm* deficiency affects DP thymocyte populations remains speculative.

The well-established requirement for *ATM* in multiple cell-cycle checkpoints raises the possibility that *Atm* might be involved in $CD3^{int}$ DP cell survival (26, 42). Another possibility is that $CD3^{int}$ DP cell loss in $Atm^{y/y}$ mice is due to down-regulation of TCR expression by means of an unknown mechanism. An intriguing possibility is a role for *ATM* in V(D)J recombination. However, transient recombination substrate studies in A-T cell lines have indicated that *ATM* does not participate directly in V(D)J recombination (43). In this context, $Atm^{y/y}$ mice generate substantial DP cell numbers (implying substantial TCRβ gene rearrangement), and our preliminary analyses revealed significant levels of TCRα rearrangements in $Atm^{y/y}$ thymocytes (data not shown). Still, it has not been determined whether the absolute rate of such chromosomal V(D)J rearrangements is equivalent to that of wild type. Therefore, while *ATM* is not required for V(D)J recombination *per se*, it may have some indirect influence on the process, a possibility consistent with the high rates of chromosomal translocations involving TCR loci in human A-T lymphocytes (27). In this regard, the $Atm^{y/y}$ phenotype, while less severe, is reminiscent of the phenotype of TCRα enhancer knockout mice (44). The latter mice have normal V(D)J recombination activity but, because of accessibility problems at TCRα locus, have reduced levels of TCRα gene rearrangement accompanied by relatively normal numbers of thymocytes, of which most are $CD3^{low}$ DP cells. Finally, another V(D)J recombination-related mechanism would involve deregulation of this activity during the cell cycle (42).

Potential Role of *Atm* in Development. The similarity between the Purkinje cell and lymphocyte abnormalities in $Atm^{y/y}$ mice and

those observed in A-T patients suggest that the consequences of *ATM* deficiency in mice and humans are substantially similar. Previous work implicated *Atm* in the regulation of IR-induced apoptosis in central nervous system (CNS) neuroblasts and DP thymocytes via a *p53*-dependent process (12, 15). However, other studies showed that *p53* deficiency does not result in the same thymocyte and CNS developmental defects that we see in $Atm^{y/y}$ mice (45, 46). In addition, individuals harboring hypomorphic mutations in *Mre11* display A-T-like clinical manifestations and cellular defects, and yet maintain a normal *p53* response (47). Therefore, *Atm* may have developmental functions separate from functions in the context of *p53*. This notion also raises the possibility that at least some cerebellar abnormalities resulting from loss of *Atm* function occur during development, rather than as a result of degeneration later in life. In the latter context, it will be of interest to determine whether the thymocyte developmental anomalies of $Atm^{y/y}$ mice contribute to generation of thymic lymphomas.

We thank Drs. Richard Gatti, Ronald DePinho, Karl Herrup, and Harvey Cantor for critical review of this manuscript. We also thank John Manis, Daniel Moheban, Dylan Stiles, and Nancy Chamberlin for advice and help. This work was supported in part by fellowships from Cancer Research Institute (to Y.G.), the Freudenberger Fund and National Institutes of Health [T32 CA09642 (to P.R.B.)], a grant from the AT Children's Project (to R.S.), and National Institutes of Health Grants NS37757 (to R.S.) and AI35714 (to F.W.A). Y.G. was an associate and F.W.A. is an investigator of the Howard Hughes Medical Institute.

1. Gatti, R. A., Boder, E., Vinters, H. V., Sparkes, R. S., Norman, A. & Lange, K. (1991) *Medicine* **70,** 99–117.
2. Boder, E. (1985) *Kroc Found. Ser.* **19,** 1–63.
3. Savitsky, K., Bar-Shira, A., Gilad, S., Rotman, G., Ziv, Y., Vanagaite, L., Tagle, D. A., Smith, S., Uziel, T., Sfez, S., *et al.* (1995) *Science* **268,** 1749–1753.
4. Banin, S., Moyal, L., Shieh, S., Taya, Y., Anderson, C. W., Chessa, L., Smorodinsky, N. I., Prives, C., Reiss, Y., Shiloh, Y., *et al.* (1998) *Science* **281,** 1674–1677.
5. Canman, C. E., Lim, D. S., Cimprich, K. A., Taya, Y., Tamai, K., Sakaguchi, K., Appella, E., Kastan, M. B. & Siliciano, J. D. (1998) *Science* **281,** 1677–1679.
6. Baskaran, R., Wood, L. D., Whitaker, L. L., Canman, C. E., Morgan, S. E., Xu, Y., Barlow, C., Baltimore, D., Wynshaw-Boris, A., Kastan, M. B. & Wang, J. Y. (1997) *Nature (London)* **387,** 516–519.
7. Shafman, T., Khanna, K. K., Kedar, P., Spring, K., Kozlov, S., Yen, T., Hobson, K., Gatei, M., Zhang, N., Watters, D., *et al.* (1997) *Nature (London)* **387,** 520–523.
8. Cortez, D., Wang, Y., Qin, J. & Elledge, S. J. (1999) *Science* **286,** 1162–1166.
9. Lavin, M. F. & Shiloh, Y. (1997) *Annu. Rev. Immunol.* **15,** 177–202.
10. Rhodes, N., D'Souza, T., Foster, C. D., Ziv, Y., Kirsch, D. G., Shiloh, Y., Kastan, M. B., Reinhart, P. H. & Gilmer, T. M. (1998) *Genes Dev.* **12,** 3686–3692.
11. Khanna, K. K., Yan, J., Watters, D., Hobson, K., Beamish, H., Spring, K., Shiloh, Y., Gatti, R. A. & Lavin, M. F. (1997) *J. Biol. Chem.* **272,** 9489–9495.
12. Herzog, K. H., Chong, M. J., Kapsetaki, M., Morgan, J. I. & McKinnon, P. J. (1998) *Science* **280,** 1089–1091.
13. Elson, A., Wang, Y., Daugherty, C. J., Morton, C. C., Zhou, F., Campos-Torres, J. & Leder, P. (1996) *Proc. Natl. Acad. Sci. USA* **93,** 13084–13089.
14. Barlow, C., Hirotsune, S., Paylor, R., Liyanage, M., Eckhaus, M., Collins, F., Shiloh, Y., Crawley, J. N., Ried, T., Tagle, D. & Wynshaw-Boris, A. (1996) *Cell* **86,** 159–171.
15. Xu, Y., Ashley, T., Brainerd, E. E., Bronson, R. T., Meyn, M. S. & Baltimore, D. (1996) *Genes Dev.* **10,** 2411–2422.
16. Soares, H. D., Morgan, J. I. & McKinnon, P. J. (1998) *Neuroscience* **86,** 1045–1054.
17. Leuzzi, V., Elli, R., Antonelli, A., Chessa, L., Cardona, F., Marcucci, L. & Petrinelli, P. (1993) *Eur. J. Pediatr.* **152,** 609–612.
18. Cabana, M. D., Crawford, T. O., Winkelstein, J. A., Christensen, J. R. & Lederman, H. M. (1998) *Pediatrics* **102,** 98–100.
19. Woods, C. G. & Taylor, A. M. (1992) *Q. J. Med.* **82,** 169–179.
20. De Leon, G. A., Grover, W. D. & Huff, D. S. (1976) *Neurology* **26,** 947–951.
21. Vinters, H. V., Gatti, R. A. & Rakic, P. (1985) *Kroc Found. Ser.* **19,** 233–255.
22. Savitsky, K., Sfez, S., Tagle, D. A., Ziv, Y., Sartiel, A., Collins, F. S., Shiloh, Y. & Rotman, G. (1995) *Hum. Mol. Genet.* **4,** 2025–2032.
23. Rho, J. H. & Sidman, R. L. (1986) *Neurosci. Lett.* **72,** 21–24.
24. Rasio, D., Negrini, M. & Croce, C. M. (1995) *Cancer Res.* **55,** 6053–6057.
25. Jacks, T., Shih, T. S., Schmitt, E. M., Bronson, R. T., Bernards, A. & Weinberg, R. A. (1994) *Nat. Genet.* **7,** 353–361.
26. Rodewald, H. R. & Fehling, H. J. (1998) *Adv. Immunol.* **69,** 1–112.
27. Taylor, A. M., Metcalfe, J. A., Thick, J. & Mak, Y. F. (1996) *Blood* **87,** 423–438.
28. Rosen, F. S. & Seligmann, M. (1993) in *Immunodeficiencies*, eds. Rosen, F. S. & Seligmann, M. (Chur, Switzerland), pp. 18–19.
29. Baurle, J. & Grusser-Cornehls, U. (1994) *Acta Neuropathol.* **88,** 237–245.
30. Gatti, R. A. & Vinters, H. V. (1985) *Kroc Found. Ser.* **19,** 225–232.
31. Paula-Barbosa, M. M., Ruela, C., Tavares, M. A., Pontes, C., Saraiva, A. & Cruz, C. (1983) *Ann. Neurol.* **13,** 297–302.
32. Liao, M. J. & Van Dyke, T. (1999) *Genes Dev.* **13,** 1246–1250.
33. Stankovic, T., Kidd, A. M., Sutcliffe, A., McGuire, G. M., Robinson, P., Weber, P., Bedenham, T., Bradwell, A. R., Easton, D. F., Lennox, G. G., *et al.* (1998) *Am. J. Hum. Genet.* **62,** 334–345.
34. Gilad, S., Chessa, L., Khosravi, R., Russell, P., Galanty, Y., Piane, M., Gatti, R. A., Jorgensen, T. J., Shiloh, Y. & Bar-Shira, A. (1998) *Am. J. Hum. Genet.* **62,** 551–561.
35. Clark, H. B., Burright, E. N., Yunis, W. S., Larson, S., Wilcox, C., Hartman, B., Matilla, A., Zoghbi, H., Y. & Orr, H. T. (1997) *J. Neurosci.* **17,** 7385–7395.
36. Rapp, M., Segev, I. & Yarom, Y. (1994) *J. Physiol. (London)* **474,** 101–118.
37. Brown, K. D., Ziv, Y., Sadanandan, S. N., Chessa, L., Collins, F. S., Shiloh, Y. & Tagle, D. A. (1997) *Proc. Natl. Acad. Sci. USA* **94,** 1840–1845.
38. Chen, G. & Lee, E. (1996) *J. Biol. Chem.* **271,** 33693–33697.
39. Watters, D., Khanna, K. K., Beamish, H., Birrell, G., Spring, K., Kedar, P., Gatei, M., Stenzel, D., Hobson, K., Kozlov, S., *et al.* (1997) *Oncogene* **14,** 1911–1921.
40. Lakin, N. D., Weber, P., Stankovic, T., Rottinghaus, S. T., Taylor, A. M. & Jackson, S. P. (1996) *Oncogene* **13,** 2707–2716.
41. Oka, A. & Takashima, S. (1998) *Neurosci. Lett.* **252,** 195–198.
42. Chao, C., Yang, E. M. & Xu, Y. (2000) *J. Immunol.* **164,** 345–349.
43. Hsieh, C. L., Arlett, C. F. & Lieber, M. R. (1993) *J. Biol. Chem.* **268,** 20105–9.
44. Sleckman, B. P., Bardon, C. G., Ferrini, R., Davidson, L. & Alt, F. W. (1997) *Immunity* **7,** 505–515.
45. Donehower, L. A., Harvey, M., Slagle, B. L., McArthur, M. J., Montgomery, C. A., Jr., Butel, J. S. & Bradley, A. (1992) *Nature (London)* **356,** 215–221.
46. Jacks, T., Remington, L., Williams, B. O., Schmitt, E. M., Halachmi, S., Bronson, R. T. & Weinberg, R. A. (1994) *Curr. Biol.* **4,** 1–7.
47. Stewart, G. S., Maser, R. S., Stankovic, T., Bressan, D. A., Kaplan, M. I., Jaspers, N. G., Raams, A., Byrd, P. J., Petrini, J. H. & Taylor, A. M. (1999) *Cell* **99,** 577–587.